When NOMA Multiplexing Meets Symbiotic Ambient Backscatter Communication: Outage Analysis

Mohamed Elsayed, *Student Member, IEEE*, Ahmad Samir, *Student Member, IEEE*, Ahmad A.Aziz El-Banna, *Member, IEEE*, Xingwang Li, *Senior Member, IEEE*, and Basem M. ElHalawany, *Senior Member, IEEE*

Abstract—**Non-orthogonal multiple access (NOMA) and ambient backscatter communication (AmBC) have gained a lot of interest as key enabling technologies in wireless communications systems. NOMA is a key player for enhancing spectrum utilization either by multiplexing multiple messages for the same user or allowing multi-users access, while AmBC shows great potential for enhancing both spectrum and energy efficiency for battery-limited devices. In this paper, the performance of a downlink NOMA multiplexing based symbiotic-radio (SR) AmBC system is analyzed over Nakagami-m fading channels. New closed-form expressions for the exact and asymptotic outage probabilities are derived. Moreover, we analyze the diversity order and the influence of the system parameters on the outage performances. Besides, we proposed a power allocation optimization technique to achieve an outage-optimal performance. Through representative Monte-Carlo simulations, we have verified the analytical results. Finally, we compared the performance of the proposed system against a benchmark OMA-based system.**

Index Terms—**Non-orthogonal multiple access, ambient backscatter communication, symbiotic radio, outage probability, power allocation, Nakagami-m fading.**

I. INTRODUCTION

Non-orthogonal multiple access (NOMA) is an efficient multiplexing technique compared with orthogonal multiple access (OMA) in achieving a better performance in terms of spectrum utilization and achievable data rates. Unlike OMA, NOMA enables many users to simultaneously access the network over the same resource block (e.g., a time slot, a frequency channel, and a spreading code) [1], [2]. NOMA has different categories including the power-domain NOMA (PD-NOMA) and code-domain NOMA, while the most widely used type is the PD-NOMA. PD-NOMA is achieved by multiplexing multiple messages with different power levels at the transmitter and using successive interference cancellation (SIC) to separate them at the receiver.

On the other hand, ambient backscatter communication (AmBC) is a recent paradigm that allows battery-free devices to send their data relying on ambient signals, such as cellular and WiFi signals [3], [4]. The main building blocks of AmBC are the ambient source, backscatter device (BD), and reader. The BD reflects the signal received from the ambient source by varying its antenna impedance [3]. As the BD needs neither dedicated power nor radio resource, AmBC is considered to be a promising technology to support low-cost and sustainable IoT devices. Another variant of the AmBC is the symbiotic

radio (SR), which is suggested in [5] for passive IoT. In SR, the power source performs a symbiotic relation with BD by powering the BD transmission, while the receiver detects the information from the source as well as the BD. The difference between AmBC and SR is that the SR not only shares the source power and the spectrum of the main transmission but also shares the receiver.

In view of the benefits mentioned above, the incorporation of AmBC or SR with NOMA could boost the performance of data conveying, energy and spectrum efficiency for massive IoT networks [6]–[9]. The coexistence of AmBC and NOMA was investigated in [10], [11], where the authors in [10] optimized the reflection coefficient at BD, the source transmitted power, and the power allocation factors at source for maximizing the ergodic capacity. The authors in [11] derived the outage probabilities (OPs) and the ergodic capacities (ECs) for a NOMA-based SR network under Rayleigh fading. In [12]–[14] the authors investigated the security of NOMA AmBC systems. In [12], the physical layer security (PLS) is investigated for ambient backscatter NOMA systems, in presence of an eavesdropper, in terms of OP and the intercept probability under hardware impairments and channel estimation errors. In [13], the effect of in-phase and quadrature-phase imbalance on the PLS of the NOMA-based AmBC systems are investigated. In [14], the reliability and security of a cognitive NOMA-based AmBC network are investigated, where the secondary transmitter and the BD communicate with the legitimate user in the existence of an eavesdropper.

In this paper, for the sake of enhancing the spectrum efficiency, we investigate a downlink NOMA-based SR-AmBC system where the source exploits NOMA multiplexing to convey two messages intended for the same destination, while simultaneously enabling a battery-free BD to send its data symbiotically. Unlike [11], the performance is investigated under Nakagami-m channel fading, a generalized distribution that can model different fading environments such as Rayleigh and one-sided Gaussian distribution for different values of m. To best of our knowledge none of previous work studied SR-AmBC based on NOMA multiplexing as an access technique in a channel characterized by Nakagami-m.

The main contributions of this paper can be summarized as follows: (1) Derive new closed-form and asymptotic expressions for the OP assuming that the wireless channels are characterized by Nakagami-m fading with an additive white Gaussian noise (AWGN). (2) Analyze the diversity order of the OPs (3) Propose and solve a power allocation optimization problem to find an outage-optimal power allocation factor. (4) Validate the analytical derivations through extensive Monte-Carlo simulations, then we study the impact of system parameters on the system outage performance. (5) Finally we carried

Mohamed Elsayed, Ahmad Samir, Ahmad A.Aziz El-Banna, and Basem M. ElHalawany are with Benha University, Egypt. Basem is the corresponding author (emails:{mohamed.elsayed, ahmed.saied, ahmad.elbanna, basem.mamdoh}@feng.bu.edu.eg), X. Li is with School of Physics and Electronic Information Engineering, Henan Polytechnic University, Jiaozuo, China (email:lixingwangbupt@gmail.com)
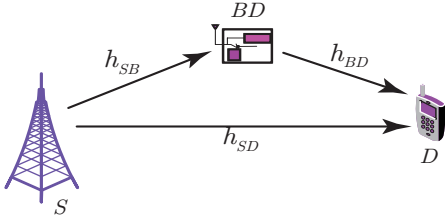
Figure 1. Downlink NOMA-based SR-AmBC system model

out a comparison between proposed system with a benchmark system.

The rest of paper is organized as follows, the system model is introduced in Section II. The performance of the considered system is analytically evaluated by deriving the OPs in Section III. The proposed power allocation algorithm is provided in Section IV. Analytical and simulation results are discussed and compared with a bench mark system in Section V. Finally, the conclusions are provided in Section VI.

II. SYSTEM MODEL

In this work, we consider the downlink NOMA-based SR-AmBC system shown in Fig.1. The system consists of a source node (S), backscatter device (BD), and a destination node (D). The transmitted power from S is used to convey its own multiplexed messages besides supporting the BD transmission simultaneously. For the sake of improving the spectrum efficiency, we assume that S adopts NOMA for multiplexing two messages, x_1 and x_2, intended for the single destination D [15], [16]. On the other hand, the BD exploits this ambient signal as a carrier of its own message x_3 by reflecting and modulating the received signal towards the same destination. The BD symbolizes a battery-free IoT device, which symbiotically coexists with S. In this work, we have assumed that the CSI is available at D. All channels are characterized by Nakagami-m fading under AWGN noise. Following the NOMA principle, the transmitted message from S to D is expressed as $x_S = \sqrt{a_1 P}\, x_1 + \sqrt{a_2 P}\, x_2$, where P denotes the total transmitted power at S, and a_i denotes the power allocation factor for the messages x_i for $i \in \{1, 2\}$. Without loss of generality, it can be assumed that $a_1 > a_2$ such that $a_1 + a_2 = 1$. Then the received signal at D is given as $y = h_{SD} x_S + \sqrt{\beta}\, h_{BD}\, h_{SB}\, x_S\, x_3 + n$, where h_{SD}, h_{SB}, and h_{BD} denote the fading of the channels with severity factor m_j and $j \in \{SD, SB, BD\}$, respectively. The expectations of the channels gains are $E\left[|h_j|^2\right] = \Omega_j$, n denotes AWGN with zero mean and σ^2 variance, and β is the BD reflection coefficient. Therefore, the received signal to interference plus noise ratio (SINR) at D to detect x_1 is given as

$$\gamma_1 = \frac{a_1 \rho |h_{SD}|^2}{a_2 \rho |h_{SD}|^2 + \beta \rho |h_{SB}|^2 |h_{BD}|^2 + 1},\qquad(1)$$

where $\rho = \frac{P}{\sigma^2}$ is the transmitted signal to noise ratio (SNR) at S. By assuming a perfect SIC, the SINR for detecting x_2 message is given as

$$\gamma_2 = \frac{a_2 \rho |h_{SD}|^2}{\beta\,\rho\,|h_{SB}|^2 |h_{BD}|^2 + 1}.\qquad(2)$$

Again D can perform another SIC assuming that $\beta < a_i$ where the SINR for detecting x_3 message is given as

$$\gamma_3 = \beta\,\rho\,|h_{SB}|^2 |h_{BD}|^2.\qquad(3)$$

Channels Distributions: Given a Nakagami-m distributed channel h_j, the channel gain, $|h_j|^2$, undergoes a Gamma distribution with probability density function (PDF) and cumulative distribution function (CDF) given respectively as follows, assuming that the fading parameter m_j is an integer value greater than or equal to one [17], [18],

$$f_{|h_j|^2}(x) = \left(\frac{m_j}{\Omega_j}\right)^{m_j} \frac{x^{m_j-1}}{\Gamma(m_j)} e^{\left(\frac{-m_j}{\Omega_j}x\right)},\qquad(4)$$

$$F_{|h_j|^2}(x) = 1 - e^{\left(\frac{-m_j}{\Omega_j}x\right)} \sum_{m=0}^{m_j-1} \frac{((m_j/\Omega_j)x)^m}{m!},\qquad(5)$$

where $\Gamma(.)$ is the gamma function. On the other hand, the PDF and CDF of the product of two squared Nakagami-m random variables, $\nu = |h_{SB}|^2 |h_{BD}|^2$, are given as follows [19] [20],

$$f_{|v|^2}(v) = \frac{2\, v^{\frac{m_{SB}+m_{BD}}{2}-1}\, K_{m_{SB}-m_{BD}}\left(\sqrt{\frac{4v}{\Omega_{SB}\Omega_{BD}}}\right)}{\Gamma(m_{SB})\Gamma(m_{BD})(\Omega_{SB}\Omega_{BD})^{\frac{m_{SB}+m_{BD}}{2}}}\qquad(6)$$

$$F_{|v|^2}(v) = 1 - \sum_{m=0}^{m_{SB}-1} \left(\frac{v}{\Omega_{SB}\Omega_{BD}}\right)^{\frac{m+m_{BD}}{2}} \frac{2K_{m_{BD}-m}\left(\sqrt{\frac{4v}{\Omega_{SB}\Omega_{BD}}}\right)}{m!\Gamma(m_{BD})},\qquad(7)$$

respectively, where $K_n(.)$ is the modified Bessel function of the second kind.

III. OUTAGE PROBABILITY ANALYSIS

In this section, we derive the OPs of the transmitted messages ($x_1, x_2,$ and x_3). The OP is defined as the probability that the SINR falls below a certain threshold value (γ_{th}). The exact and asymptotic closed-form expressions of the OPs are derived in the following subsections.

A. *Outage Probability of* x_1

The outage event of x_1 occurs if D can not decode x_1, which can be formulated as $OP_1 = 1 - \Pr(\gamma_1 > \gamma_{th})$, where $\gamma_{th} = 2^{R_{th}} - 1$ and R_{th} is the target data rate. By using (1), OP_1 can be expressed as follows

$$OP_1 = 1 - \Pr(\underbrace{|h_{SD}|^2 > (A_1 v + \frac{\tau_1}{\rho})}_{B_1}),\qquad(8)$$

where $\tau_1 = \frac{\gamma_{th}}{(a_1 - a_2\gamma_{th})}$ and $A_1 = \tau_1\beta$ such that $a_1 > a_2\gamma_{th}$. The closed-form expression of OP_1 is given in (9) at the top of next page, which is derived in the Appendix.

B. *Outage Probability of* x_2

The outage event of x_2 occurs when D can not decode x_1 or x_2 which can be formulated as $OP_2 = 1 - \Pr(\gamma_1 > \gamma_{th}, \gamma_2 > \gamma_{th})$. By using (1) and (2), we get,

$$OP_2 = 1 - \Pr(|h_{SD}|^2 > \frac{\gamma_{th}(\beta\rho v+1)}{\rho(a_1-a_2\gamma_{th})}, |h_{SD}|^2 > \frac{\gamma_{th}(\beta\rho v+1)}{a_2\rho})$$
$$= 1 - \Pr(\underbrace{|h_{SD}|^2 > A_2 v + \frac{\delta}{\rho}}_{B_2}),$$

$$\qquad(10)$$

where $\tau_2 = \frac{\gamma_{th}}{a_2}$, $\delta = \max(\tau_1, \tau_2)$, and $A_2 = \delta\beta$. Comparing B_2 with B_1, the closed-form expression of OP_2 can be found similarly as in (11) at the top of next page.

$$OP_1 = 1 - \frac{e^{\left(\frac{-m_{SD}\tau_1}{\Omega_{SD}\ \rho}\right)}}{\Gamma(m_{SB})\Gamma(m_{BD})(\Omega_{SB}\Omega_{BD})^{\frac{m_{SB}+m_{BD}}{2}}} \sum_{m=0}^{m_{SD}-1} \sum_{n=0}^{m} \left(\begin{array}{c} \binom{m}{n} \frac{(m_{SD}A_1/\Omega_{SD})^{m-(n+\frac{m_{SB}+m_{BD}}{2})}}{m!}(\frac{\tau_1}{\rho A_1})^{m-n} \\ \times G_{1,2}^{2,1}\left(\frac{\Omega_{SD}}{m_{SD}A_1\Omega_{SB}\Omega_{BD}} \ \middle| \ \begin{array}{c} 1-(n+\frac{m_{SB}+m_{BD}}{2}) \\ \frac{m_{SB}-m_{BD}}{2}, \frac{m_{BD}-m_{SB}}{2} \end{array} \right) \end{array} \right).$$
(9)

$$OP_2 = 1 - \frac{e^{\left(\frac{-m_{SD}\delta}{\Omega_{SD}\ \rho}\right)}}{\Gamma(m_{SB})\Gamma(m_{BD})(\Omega_{SB}\Omega_{BD})^{\frac{m_{SB}+m_{BD}}{2}}} \sum_{m=0}^{m_{SD}-1} \sum_{n=0}^{m} \left(\begin{array}{c} \binom{m}{n} \frac{(m_{SD}A_2/\Omega_{SD})^{m-(n+\frac{m_{SB}+m_{BD}}{2})}}{m!}(\frac{\delta}{\rho A_2})^{m-n} \\ \times G_{1,2}^{2,1}\left(\frac{\Omega_{SD}}{m_{SD}A_2\Omega_{SB}\Omega_{BD}} \ \middle| \ \begin{array}{c} 1-(n+\frac{m_{SB}+m_{BD}}{2}) \\ \frac{m_{SB}-m_{BD}}{2}, \frac{m_{BD}-m_{SB}}{2} \end{array} \right) \end{array} \right).$$
(11)

C. Outage Probability of x_3

Since x_3 is the weakest message, the receiver has to perform SIC for x_1 and x_2 to be able to decode x_3, so the outage of x_3 occurs when the system fails to decode any of the three messages, thus OP_3 represents the total system outage also, and can be formulated as $OP_3 = 1 - \Pr(\gamma_1 > \gamma_{th}, \gamma_2 > \gamma_{th}, \gamma_3 > \gamma_{th2})$, where γ_{th2} is the SINR threshold at D for detecting x_3. Substituting (1), (2), and (3) into OP_3 we get,

$$OP_3 = 1 - \Pr(|h_{SD}|^2 > (A_2v + \frac{\delta}{\rho}), v > \frac{\gamma_{th2}}{\beta\rho})$$
$$= 1 - \underbrace{\int_{\frac{\gamma_{th2}}{\beta\rho}}^{\infty} \int_{A_2v+\frac{\delta}{\rho}}^{\infty} f_{|h_{SD}|^2}(x)f_v(v)dxdv}_{B_3}.$$
(12)

Based on the analysis performed in Appendix, we can write

$$B_3 = \theta_2 \sum_{m=0}^{m_{SD}-1} \frac{(m_{SD}A_2/\Omega_{SD})^m}{m!} \sum_{n=0}^{m} \binom{m}{n}(\frac{\delta}{\rho A_2})^{m-n} \times$$
$$\underbrace{\int_{\frac{\gamma_{th2}}{\beta\rho}}^{\infty} e^{\frac{-m_{SD}A_2v}{\Omega_{SD}}} v^{n+\frac{m_{SB}+m_{BD}}{2}-1} K_{m_{SB}-m_{BD}}(\sqrt{\frac{4v}{\Omega_{SB}\Omega_{BD}}})dv}_{I_2},$$
(13)

where $\theta_2 = \frac{2e^{\left(\frac{-m_{SD}\delta}{\Omega_{SD}\rho}\right)}}{\Gamma(m_{SB})\Gamma(m_{BD})(\Omega_{SB}\Omega_{BD})^{\frac{m_{SB}+m_{BD}}{2}}}$. Using variable conversion $y = v - \frac{\gamma_{th2}}{\beta\rho}$, we can express $I_2 = \int_0^\infty e^{-y}f(y)dy$, where

$$f(y) = e^{y - \frac{m_{SD}A_2(y+\frac{\gamma_{th2}}{\beta\rho})}{\Omega_{SD}}}(y + \frac{\gamma_{th2}}{\beta\rho})^{n+\frac{m_{SB}+m_{BD}}{2}-1}$$
$$\times K_{m_{SB}-m_{BD}}(\sqrt{\frac{4(y+\frac{\gamma_{th2}}{\beta\rho})}{\Omega_{SB}\Omega_{BD}}}).$$
(14)

To the best of the authors knowledge, the integration form in I_2 is intractable. However, a tight approximation can be expressed using Gauss-Laguerre technique [21, Eq. (25.4.45)] as $I_2 = \sum_{i=1}^{k} w_i f(y_i)$, where y_i is the ith zero of the Laguerre polynomial, $L_n(x)$, while w_i is the corresponding weight $w_i = \frac{(n!)^2 x_i}{(n+1)^2[L_{n+1}(x_i)]^2}$. The final expression of OP_3 can be written as in (15) at the top of next page, where $c_1 = \Gamma(m_{SB})\Gamma(m_{BD})(\Omega_{SB}\Omega_{BD})^{\frac{m_{SB}+m_{BD}}{2}}$.

D. Asymptotic Outage Probability

To gain insight on the system performance under high SNR conditions ($\rho \to \infty$), we derive the asymptotic outage probabilities, which can be expressed as follows:

$$OP_1 \approx 1 - \frac{1-\frac{\phi_1}{\rho}}{c_1} \sum_{m=0}^{m_{SD}-1} \sum_{n=0}^{m} \psi_1(m,n)(\frac{1}{\rho})^{m-n},$$
(16a)

$$OP_2 \approx 1 - \frac{1-\frac{\phi_2}{\rho}}{c_1} \sum_{m=0}^{m_{SD}-1} \sum_{n=0}^{m} \psi_2(m,n)(\frac{1}{\rho})^{m-n},$$
(16b)

$$OP_3 \approx 1 - \frac{2(1-\frac{\phi_2}{\rho})}{c_1} \sum_{m=0}^{m_{SD}-1} \sum_{n=0}^{m} \sum_{i=1}^{k} \psi_3(m,n)(\frac{1}{\rho})^{m-n} w_i \tilde{f}(y_i),$$
(16c)

where the following approximation are assumed when ρ tends to infinity [11]: $e^{\frac{-\phi_1}{\rho}} \approx 1 - \frac{\phi_1}{\rho}$ in (9), and $e^{\frac{-\phi_2}{\rho}} \approx 1 - \frac{\phi_2}{\rho}$ in (11), and (15), $\tilde{f}(y) = e^{y(1-\phi_3)}y^{\phi_4}K_{m_{SB}-m_{BD}}(\sqrt{\phi_5 y})$, c_1, $\phi_p, p \in [1,5]$, and $\psi_q(m,n)$ for $q \in \{1,2,3\}$ are constants with respect to ρ. $\phi_1 = \frac{m_{SD}\tau_1}{\Omega_{SD}}$, $\phi_2 = \frac{m_{SD}\delta}{\Omega_{SD}}$, $\phi_3 = \frac{m_{SD}A_2}{\Omega_{SD}}$, $\phi_4 = n + \frac{m_{SB}+m_{BD}}{2} - 1$, $\phi_5 = \frac{4}{\Omega_{SB}\Omega_{BD}}$ and

$$\psi_1(m,n) = \binom{m}{n}\frac{(m_{SD}A_1/\Omega_{SD})^{m-(n+\frac{m_{SB}+m_{BD}}{2})}}{m!}(\frac{\tau_1}{A_1})^{m-n}$$
$$\times G_{1,2}^{2,1}\left(\frac{\Omega_{SD}}{m_{SD}A_1\Omega_{SB}\Omega_{BD}} \middle| \begin{array}{c} 1-(n+\frac{m_{SB}+m_{BD}}{2}) \\ \frac{m_{SB}-m_{BD}}{2}, \frac{m_{BD}-m_{SB}}{2} \end{array} \right),$$

$$\psi_2(m,n) = \binom{m}{n}\frac{(m_{SD}A_1/\Omega_{SD})^{m-(n+\frac{m_{SB}+m_{BD}}{2})}}{m!}(\frac{\delta}{A_1})^{m-n}$$
$$\times G_{1,2}^{2,1}\left(\frac{\Omega_{SD}}{m_{SD}A_1\Omega_{SB}\Omega_{BD}} \middle| \begin{array}{c} 1-(n+\frac{m_{SB}+m_{BD}}{2}) \\ \frac{m_{SB}-m_{BD}}{2}, \frac{m_{BD}-m_{SB}}{2} \end{array} \right),$$

$$\psi_3(m,n) = \binom{m}{n}\frac{(m_{SD}A_2/\Omega_{SD})^m}{m!}(\frac{1}{\beta})^{m-n}.$$

E. Diversity Order

To obtain further insights, we consider the achievable diversity order of the proposed system outage probabilities which is defined as the slope of its OP_l, and based on [22], we can calculate diversity order as $d_{OP_l} = -\lim_{\rho\to\infty}(\log(OP_l)/\log(\rho))$ where $l \in \{1,2,3\}$. It is clear from (16) that $d_{OP_l} \propto \rho^{-argmin(m-n)}$, which means $d_{OP} = argmin(m-n) = 0$ at $n = m$. This result is consistent with the plots in Fig.2 where the three OPs saturates with zero slopes.

IV. PROPOSED POWER ALLOCATION ALGORITHM

In this section, we propose a power allocation algorithm for optimizing the system OP under fixed value of the reflection coefficient β. The proposed optimization problem is given as:

$$OP_3 = 1 - \frac{2}{c_1} e^{\left(\frac{-m_{SD}\delta}{\Omega_{SD}\rho}\right)} \sum_{m=0}^{m_{SD}-1} \sum_{n=0}^{m} \binom{m}{n} \frac{(m_{SD}A_2/\Omega_{SD})^m}{m!} \left(\frac{1}{\rho\beta}\right)^{m-n} \sum_{i=1}^{k} w_i f(y_i). \qquad (15)$$

$$\min_{a_1} \; OP_3 \qquad (17a)$$

$$\text{s.t. } 0.5 < a_1 < 1 \qquad (17b)$$

$$a_1 + a_2 = 1. \qquad (17c)$$

We provide the following Theorem to solve Problem (17).

Theorem 1: *Probelm* (17) *is a convex problem and the optimal power allocation factor value is achieved at* $a_1^* = \frac{1+\gamma_{th}}{2+\gamma_{th}}$.
Proof: Given that the two constraints in (17b) and (17c) are convex, we need to prove the convexity of the objective function in (17a), which can be expressed as:

$$OP_3 = 1 - \left(\frac{2}{c_1} \sum_{m=0}^{m_{SD}-1} \sum_{n=0}^{m} \sum_{i=1}^{k} c_2 e^{-c_3\delta} \delta^m \right), \qquad (18)$$

where

$$c_2 = \binom{m}{n} \frac{(m_{SD}/\Omega_{SD})^m}{m!} \left(\frac{1}{\rho\beta}\right)^{m-n} e^y (y + \frac{\gamma_{th2}}{\beta\rho})^{n + \frac{m_{SB}+m_{BD}}{2} - 1}$$

$$\times K_{m_{SB}-m_{BD}} \left(\sqrt{\frac{4(y + \frac{\gamma_{th2}}{\beta\rho})}{\Omega_{SB}\Omega_{BD}}} \right) w_i,$$

$$c_3 = \frac{m_{SD}}{\Omega_{SD}} \left(\frac{1}{\rho} + \beta(y + \frac{\gamma_{th2}}{\beta\rho}) \right). \qquad (19)$$

By differentiating the OP_3 in (18) with respect to δ, which is a function of a_1, the derivative is given as

$$\frac{\partial OP_3}{\partial \delta} = \frac{2}{c_1} \sum_{m=0}^{m_{SD}-1} \sum_{n=0}^{m} \sum_{i=1}^{k} c_2 e^{-c_3\delta} (c_3\delta^m - m\delta^{m-1}). \qquad (20)$$

After some mathematical manipulation, we can prove that $\frac{\partial OP_3}{\partial \delta}$ in (20) is always a positive value. To find the derivative of OP_3 with respect to a_1 we can use the chain rule, then $\frac{\partial OP_3}{\partial a_1} = \frac{\partial OP_3}{\partial \delta} \times \frac{\partial \delta}{\partial a_1}$. According to the definition of $\delta = \max(\tau_1, \tau_2)$, we can divide the range into two intervals based on the value of a_1

• For $0.5 < a_1 < (1 + \gamma_{th})/(2 + \gamma_{th})$:

In this interval $\tau_1 > \tau_2$ and $\delta = \frac{\gamma_{th}}{a_1 - (1-a_1)\gamma_{th}}$, then we can write $\frac{\partial \delta}{\partial a_1} = \frac{-(1+\gamma_{th})\gamma_{th}}{(a_1(1+\gamma_{th}) - \gamma_{th})^2}$, and then, it is clear that $\frac{\partial OP_3}{\partial a_1}$ is a negative value, this result indicates a monotonically decreasing function in this interval.

• For $(1 + \gamma_{th})/(2 + \gamma_{th}) < a_1 < 1$:

In this interval $\tau_1 < \tau_2$ and $\delta = \frac{\gamma_{th}}{1-a_1}$, then we can write $\frac{\partial \delta}{\partial a_1} = \frac{\gamma_{th}}{(1-a_1)^2}$, and it is clear that $\frac{\partial OP_3}{\partial a_1}$ is a positive value. This result leads to monotonically increasing function.

Now we can notice that OP_3 is monotonically decreasing function in the range $0.5 < a_1 < \frac{1+\gamma_{th}}{2+\gamma_{th}}$, with the minimum value at the upper limit of this interval, and monotonically increasing function in the range $\frac{1+\gamma_{th}}{2+\gamma_{th}} < a_1 < 1$, and the minimum is at lower limit of this interval. So, we can conclude that OP_3 is a convex function with an optimal value at the inflection point between the two interval with outage-optimal power allocation of $a_1^* = \frac{1+\gamma_{th}}{2+\gamma_{th}}$.

Figure 6 proves the correctness of **Theorem 1** graphically. In this figure we used $\gamma_{th} = 1$ which implies that $a_1^* \approx 0.66$,

this result is exactly what we got and highlighted in Fig. 6. This solution is used as an outage-optimal power allocation scheme in the rest of this paper.

V. RESULTS AND DISCUSSIONS

In this section, we illustrate the derived OP metric, based on which some insights are highlighted. Monte Carlo simulations are generated to corroborate the proposed analysis. Unless mentioned otherwise, the simulation parameters used for generating the plots are given as [17], [23]: $\sqrt{\beta} = 0 : 1$, $a_1 = 0.5 : 1$, $\Omega_i = 0.75 : 3$, $\gamma_{th} = 1$, $\gamma_{th} = 0.1$, $m_{SD} = 4$, $m_{SB} = 1$, and $m_{BD} = 1$. To gain more insight into the system performance, we show the relations between OP and other system controlling parameters such as ρ, β, and a_1. In the following, we denote "Ana" as the analytical result, "Asym" as an asymptotic result, and "Sim" as Monte-Carlo simulation results.

Figure 2 shows the variations of the three messages' OPs versus the transmitted SNR (ρ) for $a_1 = 0.66$, $\sqrt{\beta} = 0.2$, $\Omega_{SD} = 2, \Omega_{SB} = 1$, and $\Omega_{BD} = 3$, also the figure investigates the effect of changing the fading parameters m_i from 1 to 3 on the OPs. It is noteworthy that the both analytical and simulation results coincide, which validates our analysis. Additionally, both results coincide with the asymptotic curves at high SNR, where all OPs saturate at constant values at high SNR. We can observe that all curves have the same slope = 0 at high SNR and that agree with diversity order calculated in section III-E. Additionally, it is noteworthy that the OPs are enhanced when the fading parameters increase.

To investigate the effects of changing the expectation of channels' gain Ω_i on the OPs, we introduce Fig. 3, which shows the OPs under two different sets of values for Ω_i named case 1 and case 2. In case 1, $\Omega_{SD} = 1.5, \Omega_{SB} = 0.75$, and $\Omega_{BD} = 2.25$, while in case 2 we increased their values as follows: $\Omega_{SD} = 2, \Omega_{SB} = 1$, and $\Omega_{BD} = 3$. It is noteworthy that the OPs of all messages of case 2 outperforms case 1 at low SNR values, while the opposite occurs after certain threshold SNR. The reason of this behavior is the increase of the exponential decay term with increasing ρ under the increased values of Ω_j for case 2 settings.
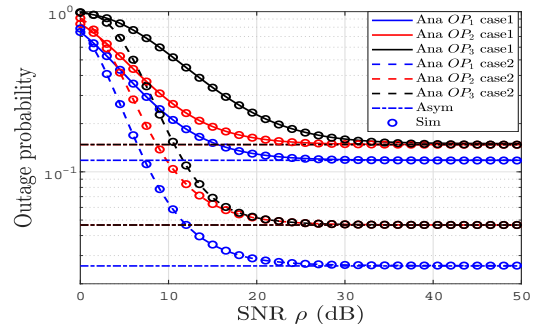
Figure 2. The OP against ρ with $a_1 = 0.66$, $\sqrt{\beta} = 0.2$, and $\Omega_{SD} = 2, \Omega_{SB} = 1, \Omega_{BD} = 3$ while in case1 ($m_{SD} = m_{SB} = m_{BD} = 1$) and case2 ($m_{SD} = m_{SB} = m_{BD} = 3$).
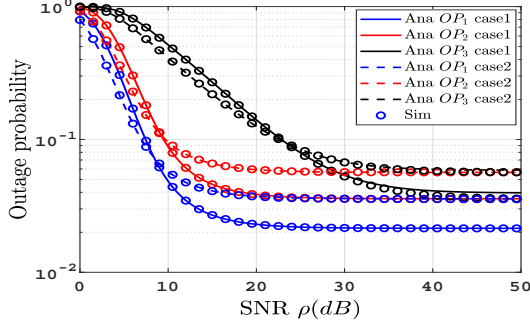
Figure 3. The OP against ρ with $a_1 = 0.66$, and $\sqrt{\beta} = 0.2$ while case1 represents $(\Omega_{SD} = 1.5, \Omega_{SB} = 0.75, \Omega_{BD} = 2.25)$ and case2 represents $(\Omega_{SD} = 2, \Omega_{SB} = 1, \Omega_{BD} = 3)$.

For more insights on the effect of the backscattering coefficient, $\sqrt{\beta}$, on the OP, Fig. 4 shows the variations of the OPs as a function of $\sqrt{\beta}$ for fixed $\rho = 40$ dB, $a_1 = 0.66$ and $\Omega_{SD} = \Omega_{SB} = \Omega_{BD} = 1$. The results show that the OPs degrade with high values of $\sqrt{\beta}$ for x_1 and x_2 since increasing $\sqrt{\beta}$ reduces their SINRs in (1) and (2). On the other hand, the OP of x_3 is enhanced as $\sqrt{\beta}$ increases up to a certain threshold, 0.11 under the given settings, and then starts to degrade again after this optimal value. The reason behind this convex behavior is that increasing the reflection coefficient reduces the SINRs of x_1 and x_2, which must be correctly decoded first according to the SIC principle of NOMA to correctly decode x_3. Consequently, there is an optimal setting for $\sqrt{\beta}$ corresponding to the optimal OP of x_3. Figure 5 compares the OPs at D for the three messages versus ρ for different values of $\sqrt{\beta}$ assuming $a_1 = 0.66$ and $\Omega_{SD} = \Omega_{SB} = \Omega_{BD} = 1$. The results shows the improvement of the OP curves with the increase of ρ up to certain values where the OPs saturates due to the increased interference levels. Additionally, smaller β leads to better outage performance of x_1 and x_2 due to the lower backscatter link interference. However, the results show that for $\sqrt{\beta}$ less than the threshold value, the OP of x_3 saturates at higher ρ.

Figure 6 shows the variations of the OPs as a function of the power allocation factor a_1 assuming $\sqrt{\beta} = 0.2$, $\rho = 25$ dB and $\Omega_{SD} = \Omega_{SB} = \Omega_{BD} = 1$. The results show that the OP of x_1 improves with the increase of a_1 due to enhancement in γ_1 under fixed β. On the other hand, the OPs of both x_2 and x_3 show a convex behavior, where the OPs in both curves improve first with the increase of a_1 up to certain optimal inflection points where both curves starts to increase.
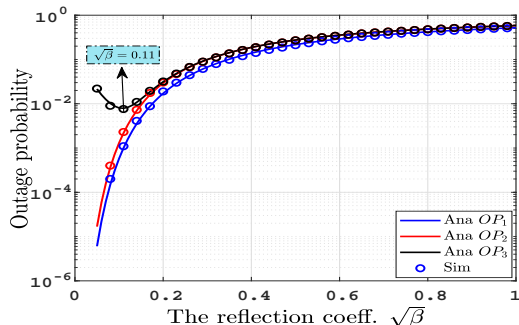
Figure 4. The OP against $\sqrt{\beta}$ at $\rho = 40$ dB and $a_1 = 0.66$.
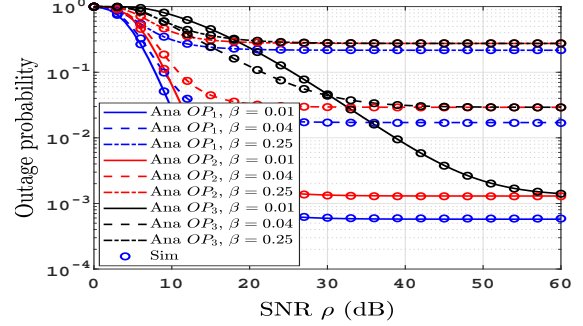
Figure 5. The OP against ρ at different β with $a_1 = 0.66$.

In the following, we evaluate the performance of the proposed system compared with a benchmark scheme; the OMA-based SR-AmBC system. Figure 7 compares the OP performance of both systems under the same system settings, $\beta = 0.04$, and $a_1 = 0.66$. According to the figure, the proposed system outperforms the benchmark in terms of both source messages, (OP_1) and (OP_2). Additionally, we can observe that the OP of BD message (OP_3) in the NOMA-system is better than that of the OMA-system up to certain threshold SNR (18 dB under those settings). Moreover, OP_3 of NOMA-based system saturates at high SNR according to the analysis in Section III-E, while, OP_3 of OMA-based system continuously improves and outperforms its counterpart.

VI. CONCLUSIONS

In this paper, we analyzed and optimized the OP of downlink NOMA-based SR-AmBC systems under Nakagami-m fading channels. We derived new analytical closed-form and asymptotic expressions for the OPs and the diversity order. Moreover, we investigated the feasibility of obtaining an outage-optimal power allocation under constant reflection coefficient. At the end of our results, we held a comparison with a benchmark system, from which we reach to an important result that our proposed system is suitable for low power Iot applications. As a future work, it is imperative to investigate a joint optimization algorithms for adjusting both the power allocation and the reflection coefficient to achieve an optimal performance. Additionally, the achievable sum ergodic capacity needs to be evaluated.
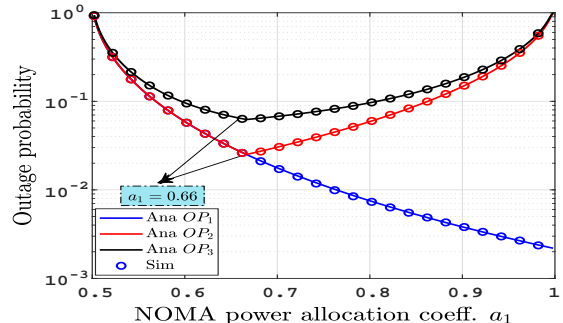
Figure 6. The OP against power allocation coeff. a_1 with $\sqrt{\beta} = 0.2$ and $\rho = 25$ dB.
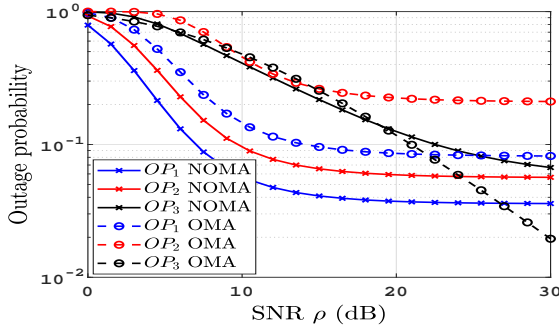
Figure 7. The Outage performance of proposed system under different schemes NOMA and OMA for $\beta = 0.04$ and $a_1 = 0.66$.

REFERENCES

[1] Z. Wei, L. Yang, D. W. K. Ng, J. Yuan, and L. Hanzo, "On the performance gain of NOMA over OMA in uplink communication systems," *IEEE Trans. Commun.*, vol. 68, no. 1, pp. 536–568, 2020.

[2] B. M. ElHalawany, F. Jameel, D. B. da Costa, U. S. Dias, and K. Wu, "Performance analysis of downlink noma systems over κ-μ shadowed fading channels," *IEEE Trans. Veh. Technol.*, vol. 69, no. 1, pp. 1046–1050, 2020.

[3] N. Van Huynh, D. T. Hoang, X. Lu, D. Niyato, P. Wang, and D. I. Kim, "Ambient backscatter communications: A contemporary survey," *IEEE Commun. Surveys Tuts.*, vol. 20, no. 4, pp. 2889–2922, 2018.

[4] B. Liu, S. Han, Z. Peng, G. Sun, and Y.-C. Liang, "A cross-layer analysis for full-duplex ambient backscatter communication system," *IEEE Wireless Commun. Lett.*, vol. 9, no. 8, pp. 1263–1267, 2020.

[5] R. Long, Y.-C. Liang, H. Guo, G. Yang, and R. Zhang, "Symbiotic radio: A new communication paradigm for passive internet of things," *IEEE Internet Things J.*, vol. 7, no. 2, pp. 1350–1363, 2020.

[6] F. Jameel, W. U. Zeb, S. A. Hassan, Z. Chang, and J. Liu, "Noma-enabled backscatter communications: Toward battery-free iot networks," *IEEE Internet of Things Mag.*, vol. 3, no. 4, pp. 95–101, 2020.

[7] W. U. Khan, M. A. Javed, T. N. Nguyen, S. Khan, and B. M. Elhalawany, "Energy-efficient resource allocation for 6g backscatter-enabled noma iov networks," *IEEE Trans. Intell. Transp. Syst.*, pp. 1–11, 2021.

[8] U. S. Toro, B. M. ElHalawany, L. WANG, and K. Wu, "Machine learning assisted signal detection in ambient backscatter communication networks," *IEEE Netw.*, vol. 68, no. 1, pp. 536–568, 2021.

[9] B. M. ElHalawany, A. A. Aziz El-Banna, and K. Wu, *Physical-Layer Security for Ambient Backscattering Internet-of-Things*. Cham: Springer International Publishing, 2021, pp. 25–37.

[10] W. Chen, H. Ding, S. Wang, D. B. da Costa, F. Gong, and P. H. J. Nardelli, "Ambient backscatter communications over noma downlink channels," *China Commun.*, vol. 17, no. 6, pp. 80–100, 2020.

[11] Q. Zhang, L. Zhang, Y.-C. Liang, and P.-Y. Kam, "Backscatter-noma: A symbiotic system of cellular and internet-of-things networks," *IEEE Access*, vol. 7, pp. 20 000–20 013, 2019.

[12] X. Li, M. Zhao, M. Zeng, S. Mumtaz, V. G. Menon, Z. Ding, and O. A. Dobre, "Hardware impaired ambient backscatter noma systems: Reliability and security," *IEEE Trans. Commun.*, vol. 69, no. 4, pp. 2723–2736, 2021.

[13] X. Li, M. Zhao, Y. Liu, L. Li, Z. Ding, and A. Nallanathan, "Secrecy analysis of ambient backscatter noma systems under i/q imbalance," *IEEE Trans. Veh. Technol.*, vol. 69, no. 10, pp. 12 286–12 290, 2020.

[14] X. Li, Y. Zheng, W. U. Khan, M. Zeng, D. Li, G. K. Ragesh, and L. Li, "Physical layer security of cognitive ambient backscatter communications for green internet-of-things," *IEEE Trans. Green Commun. Netw.*, vol. 5, no. 3, pp. 1066–1076, 2021.

[15] Y. Zhang, Z. Yang, Y. Feng, and S. Yan, "Performance analysis of cooperative relaying systems with power-domain non-orthogonal multiple access," *IEEE Access*, vol. 6, pp. 39 839–39 848, 2018.

[16] R. Ramesh, S. Gurugopinath, and S. Muhaidat, "Outage performance of relay-assisted single- and dual-stage noma over power line communications," *IEEE Access*, vol. 9, pp. 86 358–86 368, 2021.

[17] Y. Ni, Y. Liu, Q. Wang, Y. Wang, H. Zhao, and H. Zhu, "Vehicular networks under nakagami-m fading channels: Outage probability and ergodic achievable rate," *IEEE Access*, vol. 8, pp. 121 501–121 512, 2020.

[18] X. Gong, X. Yue, and F. Liu, "Performance analysis of cooperative noma networks with imperfect csi over nakagami-m fading channels," *Sens.*, vol. 20, no. 2, 2020.

[19] U. Fernandez-Plazaola, L. Moreno-Pozas, F. J. Lopez-Martinez, J. F. Paris, E. Martos-Naya, and J. M. Romero-Jerez, "A tractable product channel model for line-of-sight scenarios," *IEEE Trans. on Wireless Commun.*, vol. 19, no. 3, pp. 2107–2121, 2020.

[20] R. E. Gaunt, "Products of normal, beta and gamma random variables: Stein operators and distributional theory," 2016.

[21] M. Abramowitz and I. A. Stegun, *Handbook of Mathematical Functions with Formulas, Graphs, and Mathematical Tables*, ninth dover printing, tenth gpo printing ed. New York: Dover, 1964.

[22] B. M. ElHalawany, A. A. A. El-Banna, and K. Wu, "Physical-layer security and privacy for vehicle-to-everything," *IEEE Communications Magazine*, vol. 57, no. 10, pp. 84–90, 2019.

[23] B. Tahir, S. Schwarz, and M. Rupp, "Analysis of uplink irs-assisted noma under nakagami-m fading via moments matching," *IEEE Wireless Commun. Lett.*, vol. 10, no. 3, pp. 624–628, 2021.

[24] V. S. Adamchik and O. I. Marichev, "The algorithm for calculating integrals of hypergeometric type functions and its realization in reduce system," in *Proceedings of the International Symposium on Symbolic and Algebraic Computation*, ser. ISSAC '90. New York, NY, USA: Association for Computing Machinery, 1990.

APPENDIX

$$B_1 = \int_0^\infty \int_{A_1 v + \frac{\tau_1}{\rho}}^\infty f_{|h_{SD}|^2}(x) f_v(v) dx dv,, \tag{A.1}$$

by substituting (5), (6) into (A.1), B_1 is expressed as

$$B_1 = \int_0^\infty \left(e^{\left(\frac{-m_{SD}}{\Omega_{SD}} (A_1 v + \frac{\tau_1}{\rho}) \right)} \right) \sum_{m=0}^{m_{SD}-1} \frac{\left((m_{SD}/\Omega_{SD})(A_1 v + \frac{\tau_1}{\rho}) \right)^m}{m!}$$
$$\times \frac{2 v^{\frac{m_{SB}+m_{BD}}{2}-1} K_{m_{SB}-m_{BD}} \left(\sqrt{\frac{4v}{\Omega_{SB}\Omega_{BD}}} \right)}{\Gamma(m_{SB})\Gamma(m_{BD})(\Omega_{SB}\Omega_{BD})^{\frac{m_{SB}+m_{BD}}{2}}} dv. \tag{A.2}$$

Using binomial expansion we can get,

$$B_1 = \theta_1 \sum_{m=0}^{m_{SD}-1} \frac{(m_{SD} A_1 / \Omega_{SD})^m}{m!} \sum_{n=0}^m \binom{m}{n} \left(\frac{\tau_1}{\rho A_1} \right)^{m-n}$$
$$\times \underbrace{\int_0^\infty e^{\frac{-m_{SD} A_1 v}{\Omega_{SD}}} v^{n+\frac{m_{SB}+m_{BD}}{2}-1} K_{m_{SB}-m_{BD}} \left(\sqrt{\frac{4v}{\Omega_{SB}\Omega_{BD}}} \right) dv}_{I_1}, \tag{A.3}$$

where $\theta_1 = \frac{2 e^{\left(\frac{-m_{SD}\tau_1}{\Omega_{SD}\rho} \right)}}{\Gamma(m_{SB})\Gamma(m_{BD})(\Omega_{SB}\Omega_{BD})^{\frac{m_{SB}+m_{BD}}{2}}}$. Since I_1 in (A.3) can not be solved in terms of elementary functions, we reformulate it based on Meijer's G-functions $G_{p,q}^{m,n}$ [24, Eq. (11, 14)], as follows,

$$I_1 = 0.5 \int_0^\infty v^{n+\frac{m_{SB}+m_{BD}}{2}-1} G_{0,1}^{1,0} \left(\frac{-m_{SD} A_1 v}{\Omega_{SD}} \middle| \begin{matrix} - \\ 0 \end{matrix} \right)$$
$$\times G_{0,2}^{2,0} \left(\frac{v}{\Omega_{SB}\Omega_{BD}} \middle| \begin{matrix} - \\ \frac{m_{SB}-m_{BD}}{2}, \frac{m_{BD}-m_{SB}}{2} \end{matrix} \right) dv, \tag{A.4}$$

which can be solved using [24, Eq. (21)] as follows

$$I_1 = 0.5 \left(\frac{m_{SD} A_1}{\Omega_{SD}} \right)^{-(n+\frac{m_{SB}+m_{BD}}{2})}$$
$$\times G_{1,2}^{2,1} \left(\frac{\Omega_{SD}}{m_{SD} A_1 \Omega_{SB}\Omega_{BD}} \middle| \begin{matrix} 1-(n+\frac{m_{SB}+m_{BD}}{2}) \\ \frac{m_{SB}-m_{BD}}{2}, \frac{m_{BD}-m_{SB}}{2} \end{matrix} \right). \tag{A.5}$$

By using (A.5), (A.3),(A.1), and (8), we get OP_1 in (9), which completes the proof.